

**CFD Simulation of the Aerodynamic Drag of Personal Electric Vehicles  
(PEV)**

By

Muhammad Nur Helmi bin Hasan

ME 14770

Dissertation submitted in partial fulfilment of  
The requirement for the Bachelor of Engineering (Hons)  
(Mechanical Engineering)

JAN 2015

Universiti Teknologi PETRONAS  
Bandar Seri Iskandar  
31750 Tronoh  
Perak Darul Ridzuan

**CERTIFICATION OF APPROVAL**

**CFD Simulation of the Aerodynamic Drag of Personal Electric Vehicles (PEV)**

By

Muhammad Nur Helmi bin Hasan

ME 14770

A project dissertation submitted to the

Mechanical Engineering Programme

Universiti Teknologi PETRONAS

In partial fulfilment of the requirement for the

Bachelor of Engineering (Hons)

Mechanical Engineering

Approved by,

-----

( Azman Zainuddin )

UNIVERSITI TEKNOLOGI PETRONAS

TRONOH, PERAK

January 2015

## CERTIFICATION OF ORIGINALITY

This is to certify that I am responsible for the work submitted in this project, that the original work is my own except as specified in the references and acknowledgements, and that the original work contained here have not been undertaken or done by unspecified sources or person.

.....

(MUHAMMAD NUR HELMI)

ME 14770

Mechanical Engineering

## ABSTRACT

Personal electric vehicles (PEV) are single-occupant vehicles driven by electric motors that can be a sustainable solution for transportation for short trip. The viability of using PEV depends on its efficiency in utilizing power from the battery. Some of the power is used to move the PEV against the aerodynamic resistance or air drag. The PEV have different position and posture of the rider. As examples, Yamaha designed Passol PEV model based on the motorcycle design where the rider position is sit-on cycle and Yamaha Segway designed based on stand-on scooter model where the rider is standing position.

For this project, the study of aerodynamic drag on the design of PEV is analysed. In this circumstances, the posture of the rider also considered as the design. To conduct this study, three models of current existing PEVs with different rider postures are analysed. The types of models involved are stand-on-scooter; Yamaha Segway model, sit-on-cycle; Yamaha Passol and bike; YikeBike.

Personal electric vehicles (PEV) such as Segway, Passol and YikeBike do not have streamlined shapes and hence induce higher drag force which can cause high electric energy use by electric motor to overcome the air drag. In this study, the air drag on three different types of PEV which are stand-on-scooter, sit-on-cycle and modern bike is analysed with the aid of Computational Fluid Dynamics (CFD) software and 3D modelling in SolidWorks.

By this analysis, the comparative study on drag force of three different types of PEV at speed range of 0-50 km/h can be studied. As comparison to YikeBike, Passol has a drag reduction of 58.0%, 56.6%, 56.3%, 51.4% and 52.3% respectively for the speed from 0 to 50 km/h. As for Segway, the drag reduction is 10.3%, 16.4%, 17.0%, 14.1% and 14.5%. As conclusion, Passol has the lowest aerodynamic force induced as compared to Segway and YikeBike. Hence, Passol is the most aerodynamic model followed by Segway and YikeBike.

## ACKNOWLEDGEMENT

Praise to God Almighty for His blessing and guidance, my Final Year Project (FYP) is successfully completed. A huge appreciation to Universiti Teknologi PETRONAS and in particular, Mechanical Engineering Department for giving me the opportunity to gain as much knowledge and experience that fulfilled the university requirement.

Apart from that, I would like to convey my thankfulness to my supervisor, Mr. Azman Zainuddin, lectures and friends for all the knowledge shared, suggestions, and encouragements during the study. Thank you for always ensures I have the best opportunity to enhance my knowledge in engineering. Lastly, I would like to give my special gratitude to my family for all the supports and encouragement. Thank you for everyone which your names are not mentioned here for helping in finishing this project. Thank you and May god bless us all.

# TABLE OF CONTENTS

CERTIFICATION OF APPROVAL .....	i
CERTIFICATION OF ORIGINALITY .....	ii
ABSTRACT.....	iii
ACKNOWLEDGEMENT .....	iv
TABLE OF CONTENTS.....	v
LIST OF FIGURES .....	vi
LIST OF TABLES.....	vi
LIST OF EQUATIONS .....	vi
CHAPTER 1: INTRODUCTION .....	1
1.1 Background Study.....	1
1.2 Problem Statement .....	2
1.3 Objectives .....	3
1.4 Scope of Study .....	3
1.5 Significance of Project .....	4
CHAPTER 2: LITERATURE REVIEW .....	5
2.1 Governing Equations .....	5
2.2 Related Previous Study .....	6
CHAPTER 3: METHODOLOGY .....	8
3.1 Project Flow Chart .....	8
3.2 Project Gantt Chart .....	9
3.3 Numerical Simulations: Computational Settings and Parameters .....	10
3.3.1 Computational Geometry and Domain .....	10
3.3.2 Boundary Conditions .....	12
3.3.3 Governing Equations and Solver Settings.....	14
CHAPTER 4: RESULTS AND DISCUSSION .....	15
4.1 Coefficient and drag force.....	15
4.2 Analysis of Pressure Field .....	19
CHAPTER 5: CONCLUSION AND RECOMMENDATION.....	22
5.1 Conclusion .....	22
5.2 Recommendation .....	23
REFERENCES .....	vii
Appendix A: Pressure Coefficient vs Velocity .....	viii
Appendix B: Turbulence Intensity Contour of YikeBike .....	ix
Appendix C: Turbulence Intensity Contour of Segway .....	x
Appendix D: Turbulence Intensity Contour of Passol .....	xi

## LIST OF FIGURES

Figure 1: Three cyclist positions UP, DP, TTP.....	6
Figure 2: Drag reduction for cyclist for UP, DP and TTP .....	7
Figure 3: Process flow chart of the project .....	8
Figure 4: Dimension of the models. (a) Passol; (b) Segway; (c) YikeBike; (d) dummy .....	10
Figure 5: Meshing elements and nodes of the models .....	11
Figure 6: Computational domain and boundary condition for simulations (in metre).....	12
Figure 7: Graph of drag force vs velocity of the models .....	16
Figure 8: Bar chart of drag force vs velocity of the models.....	16
Figure 9: Turbulent intensity contour of Segway at 50 km/h .....	18
Figure 10: Turbulent intensity contour of YikeBike at 50 km/h.....	18
Figure 11: Pressure coefficient contour at 50 km/h. (a) Passol; (b) Segway; (c) YikeBike....	19
Figure 12: Pressure coefficient on mid cross section plane .....	20
Figure 13: Pressure drag force induce by the models respect to velocity .....	21

## LIST OF TABLES

Table 1: Project Gantt chart FYP I and FYP II.....	9
Table 2: Meshing parameter ANSYS .....	11
Table 3: Boundary condition and fluid properties .....	13
Table 4: Pressure-velocity coupling solution method.....	14
Table 5: Drag result and coefficient.....	15
Table 6: Drag area of the models .....	17
Table 7: Wind tunnel and CFD comparison .....	23

## LIST OF EQUATIONS

Equation 1: Total power consumption on electric vehicle.....	5
Equation 2: Power to overcome air drag.....	5
Equation 3: Drag force equation.....	6
Equation 4: Pressure coefficient.....	19
Equation 5: Drag force coefficient.....	22

## CHAPTER 1: INTRODUCTION

### 1.1 Background Study

Personal Electric Vehicle (PEV) is used as a short distance trip transportation like going to train or bus station especially for those who are living in urban area. Due to beneficial effect on environment, PEVs are an important factor for improvement of traffic and more practically for a healthier environment [1]. PEV is a vehicle with a single passenger operated by electric motor and electric power stored in battery as the main source. Traveling at long distance is a limitation of PEV since the battery have limited energy storage capacity. As an example, lithium ion have a power density of 500 W/kg, discharge rate of 448 kJ/kg which contribute to a travel distance only up to 10 km per single charge. Due to this limitation, the usage of stored electric power need to be optimize.

The power required at the wheels of vehicle can be modelled as the sum of the power required to overcome the rolling resistance, the power to overcome air drag, the power associated with climbing or descending the slope, and the power associated with accelerating and decelerating the vehicle [2]. For this study, the assumption is made where the PEV moves at a constant speed on a flat surface neglecting the effect of rolling resistance. Hence, leaving only the air drag effect as the scope of this study. The aerodynamic study on the design is carried out to determine the drag force induced by three different models.

For bicycle at racing speed (about 54 km/h in time trials), the aerodynamic resistance or drag is about 90% of the total resistance [3]. Note that, the projected area compute in this drag study is based on PEV's design and human dummy postures. Basically, the size of PEV is smaller compared to average adult human size. The posture of user itself contribute more than 50% of the frontal area and

the remainder cause by the PEV body design. Based on (2), frontal area is one of the factors contribute to air drag. The higher the frontal area, the higher the power needed to overcome the air drag. While the important of reducing aerodynamic drag of car is well known and researched, the case of air drag on PEV has received less attention.

## 1.2 Problem Statement

The increase demand of electric vehicle has push the development of PEV to be more practical and reliable transportation. In this project, air drag is the main issues to be addressed. The viability of using PEV depends on its efficiency in utilizing power from the battery. Some of the power is use to move the PEV against the aerodynamic resistance or air drag. Since, PEV have poor streamline and less aerodynamic. At high speed, the air drag become dominant and contribute to a high usage of electric power to overcome the drag especially during accelerating and decelerating. Subsequently, it will limit the travel distance of PEV since the battery has limitation in storage capacity.

For PEV, most of the projected area is contributed by rider body. The posture of a rider depends on the designed PEV. Hence, posture of the rider itself play a major role in the air drag. Besides that, the main body frame of PEV need to be consider in the air drag analysis as well. So far, less attention has been given by researchers in overcoming the air drag on PEV since PEV move at low speed and induce less air drag compared to other vehicles.

### 1.3 Objectives

The objective of this project are:

- a) To analyse the air drag on PEV using Computational Fluid Dynamic (CFD) method which involved external flow of fluid around model. In this project, the air drag simulation performed focus on the rider posture and PEV main body frame
- b) To carry out comparative study on the aerodynamic drag of stand-on scooter (Segway), sit-on cycle (Passol) and modern bike (YikeBike).

### 1.4 Scope of Study

- a) Three types of PEV are use in CFD analysis. Stand-on-scooters (Yamaha Segway), sit-on cycle (Yamaha Passol) and modern bike (YikeBike).
- b) The speeds of PEV covered in this study are 0-50 km/h
- c) The size of human dummy is set constant throughout the simulation.
- d) The CFD simulation is carried out by using ANSYS fluent, external fluid flow and model generated by SolidWorks.
- e) The assumption of fluid flow is made where:

- a. Steady fluid flow,

$$\frac{\partial}{\partial t} = 0$$

- b. Incompressible flow,  $\rho_{air} = constant$

- c. Viscous fluid,  $\mu \neq 0$

- d. No pressure gradient in the flow direction,  $\frac{\partial p}{\partial z} = 0$

### 1.5 Significance of Project

By conducting this project, the drag force caused by fluid dynamic drag and skin friction on 3 different models of PEV at the speed between 0-50 km/h can be obtained by CFD simulation. This analysis is beneficial to PEV designer and manufacturer since they can use this data to conduct further analysis in reducing the air drag on PEV. It would provide some guideline on how to perform the external fluid flow analysis using CFD tools. This will lead to enhancement of performance and energy optimization for PEV.

The usage of the real wind tunnel can now be made possible by using CFD software. It is also expected to give better understanding on fluid flow. In addition, this analysis may help the future research of air drag on PEV design. This may lead to further study on this matter resulting in detail and expansion of knowledge regarding this topic.

## CHAPTER 2: LITERATURE REVIEW

### 2.1 Governing Equations

In the previous study [4] the total power required to overcome force acting on electric vehicle is analysed.

The equations are stated below:

$$P_{total} = \frac{P_{acc} + P_{slope} + P_{Drag} + P_{Friction}}{\eta_{motor} \cdot \eta_{trans}} + P_{Aux(radio, etc)} \quad (1)$$

$$P_{Drag} = \frac{1}{2} \rho C_d A (v - v_{wind})^3 \quad (2)$$

Equation 1 represent the total power required to overcome the forces acting over the vehicle considering the motor and transmission efficiency and the auxiliary power required for the radio, lights etc. [4]. The total power to overcome the force acting over vehicle is increase as the air drag increase assuming other variables are constant. The power required at the wheels are determined by the basic physics of moving a wheeled vehicle over the road surface and through air. At low speeds, rolling resistance dominates the power requirement and at high speeds, air drag dominate [2] .

The result [4] shows that, the power required to overcome the air drag increase exponentially as the speed of the electric vehicle increase (2). As the speed increase, the gradient of the air drag become stepper resulting in domination of air drag at a high speed. This also can be proved by Equation 2 where  $C_d$  the drag coefficient,  $\rho$  is the air density,  $A$  is the vehicle frontal area,  $v$  and  $v_{wind}$  correspond to the vehicle and wind velocity respectively [4]. Based on Equation 3, the higher the net velocity of vehicle and wind, the higher the drag force. Nevertheless, the frontal area of a vehicle also one of the factors affecting the air drag. The frontal area of a vehicle is directly proportional to power required to overcome the air drag.

To analyse the aerodynamic drag acting on the PEV, the equation is defined as shown (3)

$$F_d = AC_d \frac{\rho U_\infty^2}{2} \quad (3)$$

The aerodynamic drag is often quantified by the drag area  $AC_d$  ( $m^2$ ), which is the product of frontal area ( $m^2$ ) and drag coefficient ( $C_d$ ). This equation basically relates the drag force  $F_d$  to the dynamic pressure ( $\frac{\rho U^2}{2}$ ).  $\rho$  is the density of air ( $kg/m^3$ ) and  $U_\infty$  is the approach-flow air speed (m/s). As for Equation 3, the drag force increase as the frontal area increase considering other variable constant. From this, the drag force at different speed of vehicle can be determine.

## 2.2 Related Previous Study

Based on previous research, the aerodynamic study on cyclist is conducted [5]. The aerodynamic drag of the cyclists is analyse using CFD simulation supported by wind-tunnel measurement. In this research [5], the positions of the cyclists during simulation is defined which are upright position (UP), dropped position (DP) and time trial position (TTP) as shown Figure 1.

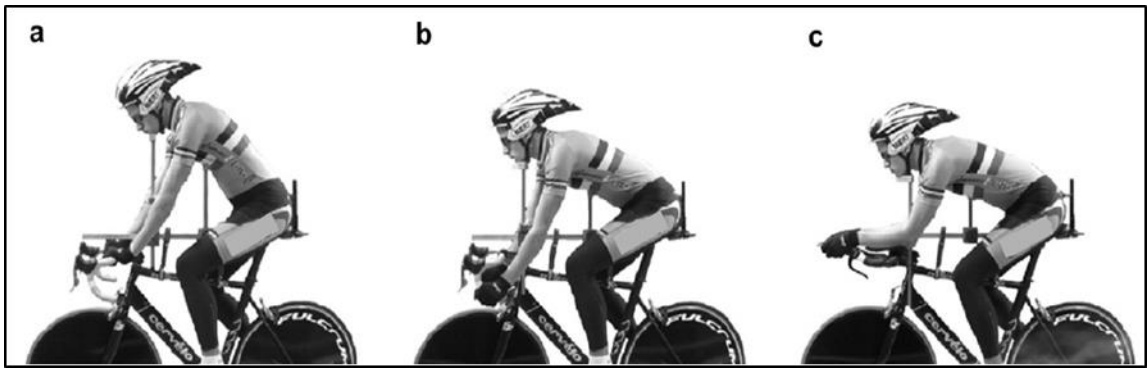


Figure 1: Three cyclist positions (Person A): (a) upright position (UP); (b) dropped position (DP); (c) time-trial position (TTP).

The distance separation for single cyclist (isolated) and drafting cyclist is varies from 0.01 m to 1 m. As the result, for single cyclist (isolated) with separation distance  $d=0.01m$ , the drag reduction of trailing cyclist for UP, DP and TTP is 27.1%, 23.1%, 13.8% respectively. While for drag reduction of leading cyclist is 0.8%, 1.7%, 2.6% for UP, DP and TTP respectively as shown in Figure 2. The drag reduction decrease with increasing separation distance [5]

This research also compared the analysis done by CFD with wind-tunnel measurement. As example, for leading cyclist with  $d=0.15\text{m}$ , the measured drag reduction was 1.6% in wind tunnel measurement and 1.3% in CFD analysis. However, the wind-tunnel experiment will not be conducted in PEV air drag study. The CFD simulation are used to describe the aerodynamic drag effects by means of detailed pressure distribution on and around the cyclist [5]. As conclusion from

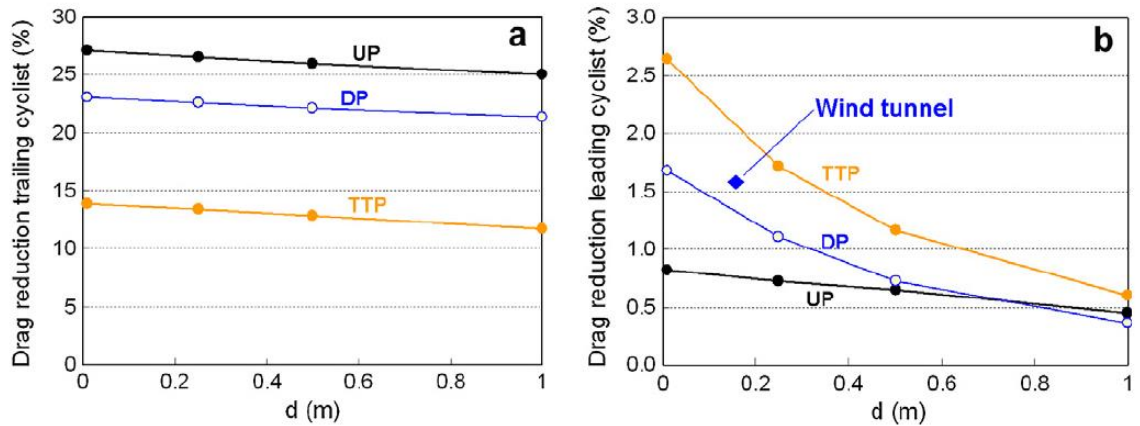


Figure 2: (a) Drag reduction for trailing cyclist for UP, DP and TTP; (b) drag reduction for leading cyclist for UP, DP and TTP and wind tunnel measurement result for DP.

this paper, both drafting cyclists significantly affect the pressure distribution on each other's body and static pressure in the region between them. The area of under pressure behind the leading cyclist interrelates with the area of overpressure in front of the trailing cyclist, which results in a reduction of the under pressure area behind the leading cyclist [5]. The overpressure area in front of the trailing cyclist gets less extended in the vertical axis but more extended in the horizontal axis, and it moves closer to the leading cyclist as the position of the cyclists changes from UP over DP to TTP.

## CHAPTER 3: METHODOLOGY

### 3.1 Project Flow Chart

Figure 3 shows the project flow chart of the study. Since there is no specific guideline in doing the research, the project method is based on previous research papers and the value of modified parameter is select based on suitable condition that fit this study.

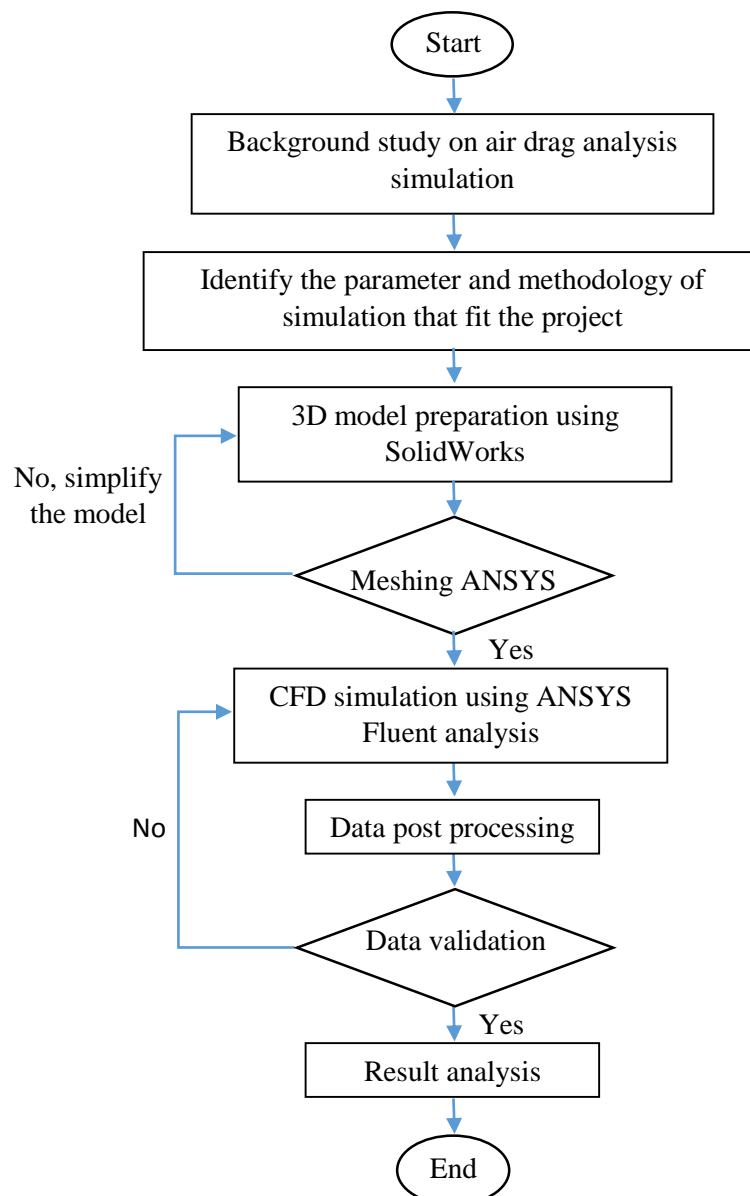


Figure 3: Process flow chart of the project

### 3.2 Project Gantt Chart

Table 1: Project Gantt chart FYP I and FYP II

FINAL YEAR PROJECT I															
NO	TASK	WEEK													
		1	2	3	4	5	6	7	8	9	10	11	12	13	14
1	Title selection & allocation														
2	Project introduction														
3	Preliminary study on PEV and air drag														
4	Review on literature														
5	Identify the general issues														
6	Review the whole concept of air drag														
7	Identifying objectives and problem														
8	Develop method of analysis														
9	Familiarise with Ansys and SolidWorks														
10	Dimension analysis of PEV														
11	Develop the 3D model on SolidWorks														
FINAL YEAR PROJECT II															
NO	TASK	WEEK													
		1	2	3	4	5	6	7	8	9	10	11	12	13	14
1	Develop the 3D model (SolidWorks)														
2	Establish simulation parameter														
3	Run simulation on Ansys														
4	Analyze the result of simulation														
6	Project work continue (Documentation)														

### 3.3 Numerical Simulations: Computational Settings and Parameters

To analyse the aerodynamic drag effects of three different designs of PEV, CFD simulations with 3D model is carried out. To the best of our knowledge, CFD studies on PEV with real rider geometries have not yet been published. The main reason to apply CFD is that it simultaneously provides information on the aerodynamic drag and on the detailed airflow pattern around the model, which can explain the drag mechanism and lead to increased insight in the fluid mechanics on PEV design.

#### 3.3.1 Computational Geometry and Domain

For the models generating, the dimension of main body frame of Segway, Passol and YikeBike are not provided in the sources since it is a confidential matter. However, the width, length and height of the overall design is provided [6] [7] [8]. Hence, the drawing done is not based on the actual dimension. Only estimation is made for every main body frame of the models. The overall dimension of the PEV and the rider is shown in Figure 4. The models drawn are in 3D with metre as dimension unit. The drawing of the models will focus more on the design shape of the model and posture of the rider. Next, the models will be import to ANSYS software in the form of STEP file for air drag simulations.

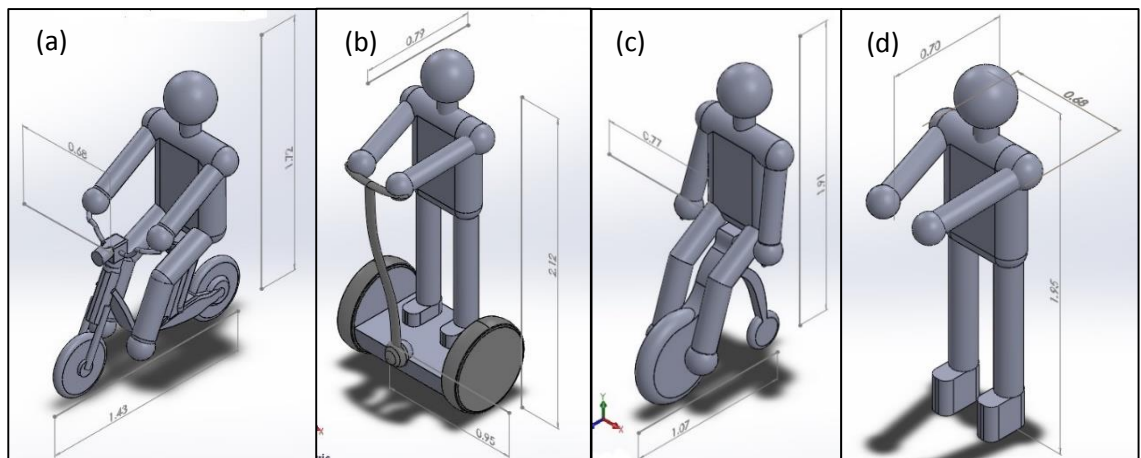


Figure 4: Dimension of the models. (a) Passol; (b) Segway; (c) YikeBike; (d) Human dummy as rider

Table 2: Meshing parameter ANSYS

PARAMETER	SPECIFICATION	VALUE
<b>Sizing</b>	Min size	0.002m
	Proximity min size	0.002m
	Max face size	0.5
	Growth rate	1.2
<b>Inflation</b>	Transition ratio	0.77
	Maximum layers	5
	Growth rate	1.2
<b>Mesh metric</b>	Average element quality	0.83
<b>No. of nodes</b>	Segway	339505
	Passol	202501
	YikeBike	122831
<b>No. of elements</b>	Segway	1861024
	Passol	1082972
	YikeBike	648233

To reduce the processing time for simulations, the model is cut into half in x-axis so that only half of the model will be used for simulations. Due to this, the number of iterations for continuity equation, x, y, z velocity equations and k-epsilon equation is reduce from below 5000 to less than 500. The models are then undergone mesh generation by using tetrahedron method for cell generation. Table 2 shows the meshing parameter for simulations. The average meshing elements quality for all models is 0.83 which is good because the highest quality is 1.00. The number of nodes and elements for every model is accepted between ranges 0.8 to 1.0. High number of nodes and elements, give significant effect to the precision of result. However, it will takes longer time to simulate. The growth rate for the meshing is 1.2 which explain the decrease in size of element as it reach the surface of model as shown in Figure 5. The size of the human dummy is set constant.

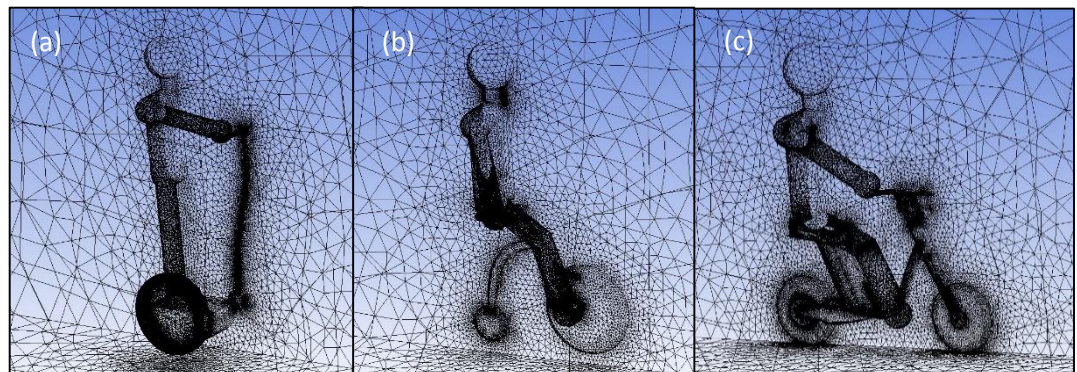


Figure 5: Meshing elements and nodes of the models. (a) Segway; (b) YikeBike; (c) Passol

### 3.3.2 Boundary Conditions

The source of the wind is at the inlet wall defined on the wind tunnel with the speed of wind from 0 to 50 km/h. In this simulations, since the PEV is in static condition, the wind speed is define as the speed of the PEV in real situation. The gap between front face of PEV is 2.5 metre from the inlet wall enough for the wind to flow at steady condition before flowing through external surface of model. The gap is set constant for all models to ensure the consistency of the simulations. For the inlet and outlet boundary condition, the turbulent kinetic energy and turbulent dissipation rate is set constant for all models which are  $1m^2/s^2$ ,  $1m^2/s^3$  respectively.

The model body surface is set to no-slip boundary wall with zero roughness. For the bottom, side and top of wind tunnel, the domain is set to be no-slip wall boundary. To simplify the simulations, the models is cut into half in x-axis in order to reduce the number of iterations. The cross section plane is set to be symmetry wall where the wall is assume to be slip. Slip wall assume that the normal velocity component and the normal gradient at the boundary are zero, generated flow parallel to the boundary [5]. For outlet computational domain, ambient static pressure was imposed. The size of wind tunnel is based on previous study on aerodynamic drag of cyclist [5] where the rule of thumb is implied as shown in Figure 6.

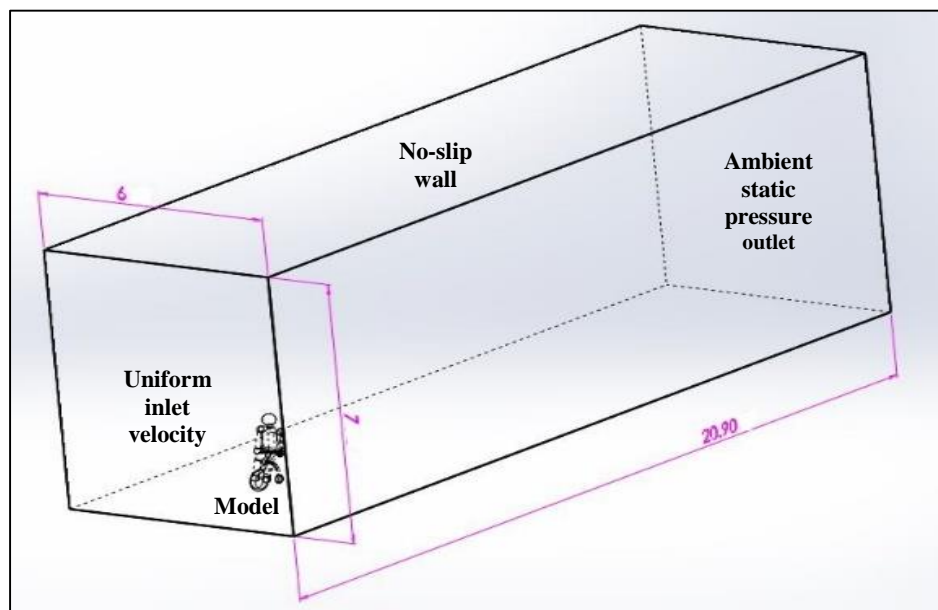


Figure 6: Computational domain and boundary condition for simulations (in metre)

Table 3: Boundary condition and fluid properties

BOUNDARY	PARAMETER	VALUE
Inlet (Velocity inlet)	Specification method	K and epsilon
	Velocity magnitude	0-50km/h
	Initial Gauge pressure	0
	Turbulent kinetic energy	1 m <sup>2</sup> /s <sup>2</sup>
	Turbulent dissipation rate	1 m <sup>2</sup> /s <sup>3</sup>
Model (wall)	Wall motion	Stationary wall
	Shear condition	No slip
	Roughness height	0
	Roughness constant	0.5
Side, top, bottom wind tunnel (wall)	Wall motion	Stationary wall
	Shear condition	No slip
Middle cross section (symmetry)	Wall motion	Slip wall
	Flow parameter	Parallel
Outlet (pressure outlet)	Specification method	K and epsilon
	Backflow direction	normal to boundary
	Gauge pressure	0
	Turbulent kinetic energy	1 m <sup>2</sup> /s <sup>2</sup>
	Turbulent dissipation rate	1 m <sup>2</sup> /s <sup>3</sup>
Fluid properties	Density(kg/m <sup>3</sup> )	1.225
	Viscosity(kg/m-s)	1.79E-05

Table 3 shows the boundary condition specifications and fluid properties used in simulations. A steady state condition is implied where the velocity, pressure and temperature are assumed to be equal at every point in the wind tunnel and does not change with time. The air density is set constant to reduce the variables in simulation, which also accommodates the parameters made by selecting steady state.

### 3.3.3 Governing Equations and Solver Settings

The simulation is ran based on 3D steady Reynolds-averaged Navier-stokes (RANS) equations which being solved by Realizable k-epsilon model with near wall modelling. K-epsilon model is chose based on previous extensive validation study, where [9] showed that k-epsilon model is the most accurate solver in predicting the aerodynamic drag, with under estimation of 4% compared to the wind tunnel test. “Realizable” means that the model fulfils certain mathematical constraints on the normal stresses, constant with the fluid mechanics of turbulent flows [10].

As comparison to Standard k-epsilon model, Realizable k-epsilon model more precisely predicts the distribution of the dissipation rate of flat and round model and also provide a better prediction of the boundary layers characteristics in a large pressure gradient, separated and recirculating flows [10]. Pressure velocity coupling is computed by Semi-Implicit Method for Pressure Linked Equations (SIMPLE) algorithm as shown in Table 4. SIMPLE algorithm is a broadly used mathematical procedure to solve the Navier-Stokes equations in CFD [11]. SIMPLE algorithms is chose based on previous CFD simulation research [5] where velocity, pressure, and density of air is the variables used to compute the air drag study.

Table 4: Pressure-velocity coupling solution method

<b>PARAMETER</b>	<b>COMPUTE METHOD</b>
Scheme	SIMPLE
<b>Spatial Discretization</b>	
Gradient	Least Square Cell Based
Pressure	Standard
Momentum	First order upwind
Turbulent kinetic energy	First order upwind
Turbulent dissipation rate	First order upwind

Convergence was monitored and the iterations were terminated when all residuals showed no further reduction with increasing number of iterations. In this study, the convergence is monitored to 0.001 for all residuals.

## CHAPTER 4: RESULTS AND DISCUSSION

### 4.1 Coefficient and drag force

In general, aerodynamic drag is affected by pressure drag arise because of the shape of the object, skin friction drag arises from the interaction between fluid and the skin of the body, interference drag result from air flow around the object which related to turbulent, lift drag or known as downforce and lastly wave drag which cause by object moving at transonic and supersonic speed due to presence of shockwave.

PEV does not have streamlined and aerodynamic shape and move at speed up to 50 km/h induced very small value of lift force and interference drag force which are neglected in this study. Apart from that, wave drag also is neglected in this study since PEV move at low speed leaving only pressure drag and skin friction drag. The data of the drag force is shown in Table 5.

Table 5: Drag result and coefficient

Model	Velocity (km/h)	Pressure force (N)	Viscous force (N)	Drag force (N)	Pressure force coef $c_p$	Viscous force coef $c_s$	Drag force coef $c_p + c_s = c_d$
Segway	0	0.00	0.00	0.00	-	-	-
	10	2.32	0.10	2.42	0.98	0.04	1.02
	20	7.51	0.29	7.80	0.79	0.03	0.82
	30	15.60	0.58	16.18	0.73	0.03	0.76
	40	26.50	0.92	27.42	0.70	0.02	0.73
	50	40.31	1.34	41.65	0.68	0.02	0.70
Passol	0	0.00	0.00	0.00	-	-	-
	10	1.63	0.06	1.69	0.69	0.03	0.72
	20	5.60	0.19	5.80	0.59	0.02	0.61
	30	11.73	0.38	12.11	0.55	0.02	0.57
	40	20.02	0.64	20.66	0.53	0.02	0.55
	50	30.38	0.94	31.32	0.51	0.02	0.53
YikeBike	0	0.00	0.00	0.00	-	-	-
	10	2.61	0.06	2.67	1.10	0.02	1.13
	20	8.90	0.18	9.08	0.94	0.02	0.96
	30	18.57	0.36	18.93	0.87	0.02	0.89
	40	30.70	0.58	31.28	0.81	0.02	0.83
	50	46.85	0.85	47.70	0.79	0.01	0.81

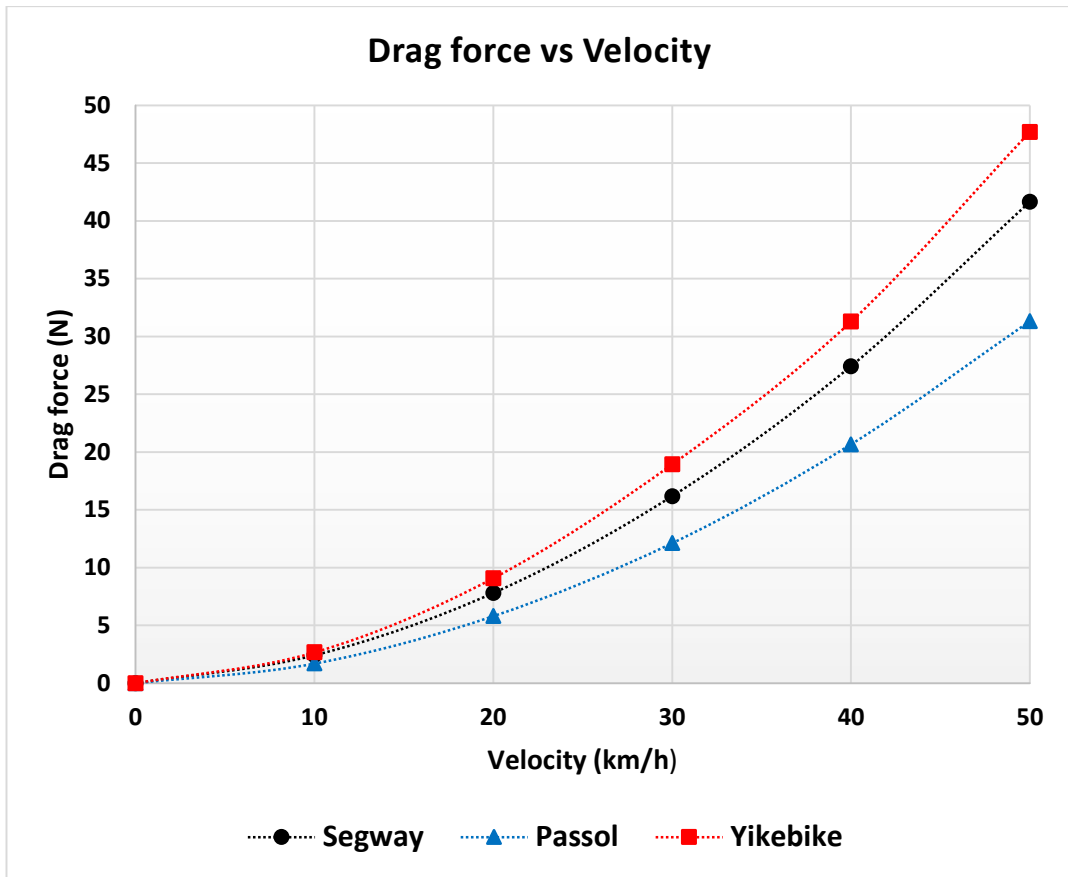


Figure 7: Graph of drag force vs velocity of the models

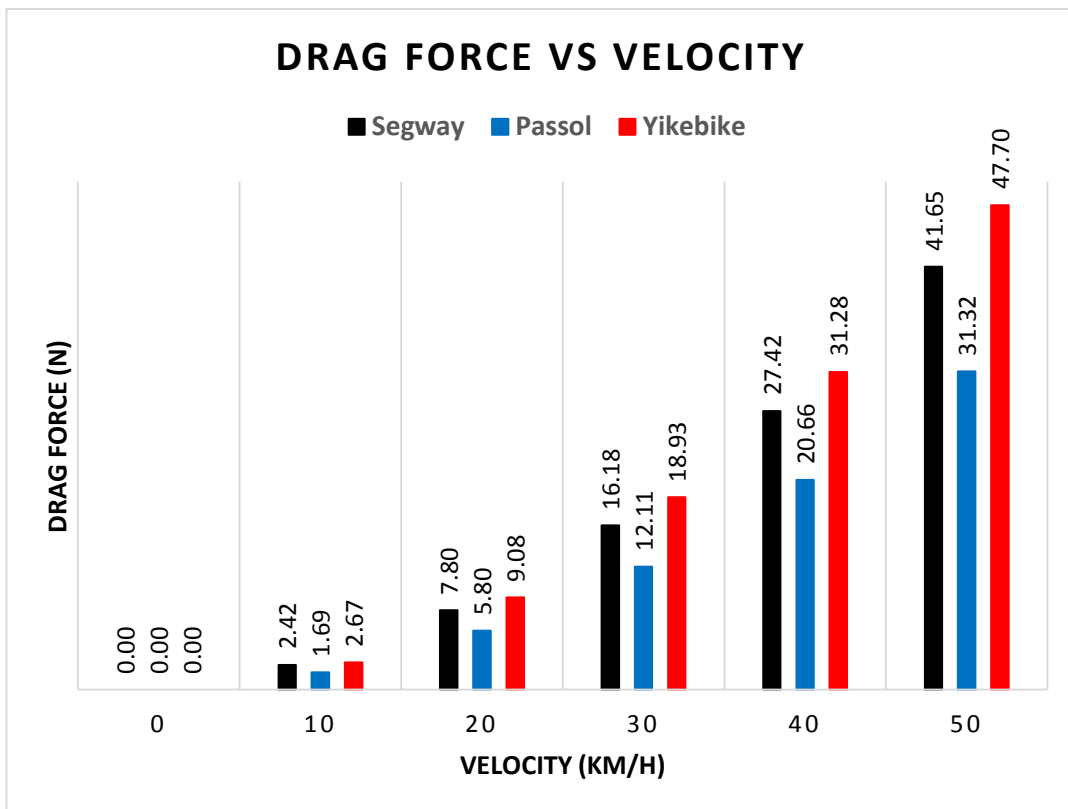


Figure 8: Bar chart of drag force vs velocity of the models

Figure 7 shows the difference in drag force induced for models at speed from 0 to 50 km/h. From the graph, it is clearly shown that, Passol model induced smallest drag force for all speeds followed by Segway and YikeBike. The highest drag force induced by the model is at at 50 km/h which are 47.7 N for YikeBike, 41.6 N for Segway and 31.3 N for Passol. The drag forces induced increase exponentially with increase in velocity as describe by Equation 3. In other words the gradient of the aerodynamic drag for every model increases as the speed of PEV increase.

As compared to YikeBike, Passol have a drag reduction of 58.0%, 56.6%, 56.3%, 51.4% and 52.3% for the speeds of 10 km/h, 20 km/h, 30 km/h, 40 km/h and 50 km/h respectively. For Segway, the drag reduction is 10.3%, 16.4%, 17.0%, 14.1% and 14.5% respectively as compared to YikeBike. Passol model have the highest drag force reduction as compared to Segway and YikeBike as shown in Figure 8 which prove that, Passol is the most aerodynamic model followed by Segway and YikeBike.

The difference in aerodynamic drag is contributed by the different in effective frontal area known as drag area which is computed by the product of projected area and coefficient of drag as shown in Equation 3. The lowest effective frontal area is Passol, followed by YikeBike and Segway as shown in Table 6.

Table 6: Drag area of the models

Model	Velocity (km/h)	Projected area (m <sup>2</sup> )	Drag force coef	Ac <sub>d</sub>
Segway	0	1.07	0.00	0.00
	10	1.07	1.02	1.09
	20	1.07	0.82	0.88
	30	1.07	0.76	0.81
	40	1.07	0.73	0.77
	50	1.07	0.70	0.75
Passol	0	0.80	0.00	0.00
	10	0.80	0.72	0.57
	20	0.80	0.61	0.49
	30	0.80	0.57	0.45
	40	0.80	0.55	0.43
	50	0.80	0.53	0.42
Yikebike	0	0.94	0.00	0.00
	10	0.94	1.13	1.06
	20	0.94	0.96	0.90
	30	0.94	0.89	0.84
	40	0.94	0.83	0.78
	50	0.94	0.81	0.76

From Table 6, the frontal area (A) of the Segway is greater than YikeBike hence induced higher drag force. However, the result shown in Figure 7 shows that YikeBike induced higher drag force for all speeds as compared to Segway. This explain the effect of resistance due to the fluctuating and irregular nature of turbulence formed when the layer of the fluid move smoothly past each other as shown in Figure 9 and Figure 10.

YikeBike have a higher maximum value of turbulent intensity of 32.9% as compared to Segway, 26.1%. From Figure 10, YikeBike induce highest turbulence intensity region which occurs between the front and rear tyre. The turbulent contour area around Segway is smaller as compared to YikeBike (refer appendices B, C, D). High turbulent intensity will add resistance to the moving object which give significant increase in total aerodynamic drag. However, the detail study on the behaviour of turbulence will not be covered in this study.

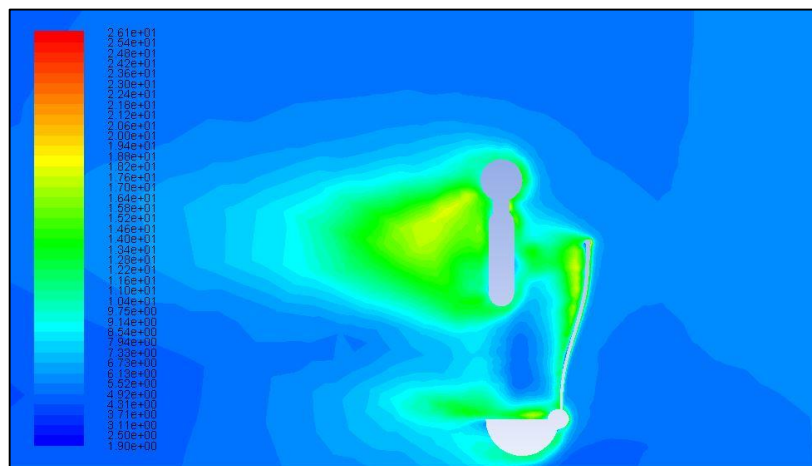


Figure 9: Turbulent intensity contour of Segway at 50 km/h

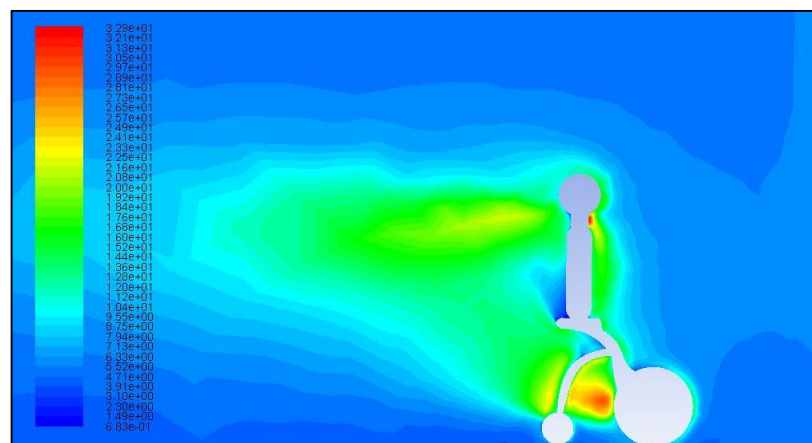


Figure 10: Turbulent intensity contour of YikeBike at 50 km/h

## 4.2 Analysis of Pressure Field

The coefficient of pressure  $C_p$  is defined as:

$$C_p = 2 \frac{P - P_o}{\rho U_\infty^2} \quad (4)$$

$P$  is the static pressure.  $P_o$  is the reference static pressure which equal to atmospheric pressure,  $\rho$  density of fluid flow and  $U_\infty$  is the speed of the object.

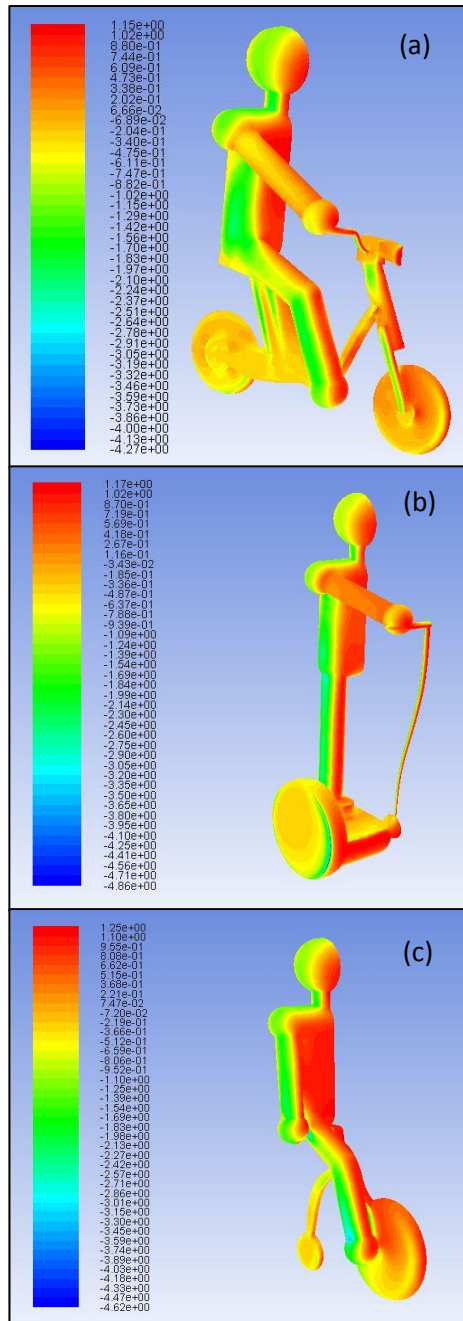


Figure 11: Pressure coefficient contour at 50 km/h. (a) Passol; (b) Segway; (c) YikeBike

From Figure 11, the contour of pressure distribution around the model can be seen where the highest pressure is formed at the frontal area and the lowest pressure is formed at the side of the model. This explain the Bernoulli's principle where for an inviscid flow of non-conducting fluid, an increase in the speed of the fluid occurs simultaneously with a decrease in pressure.

High pressure is formed on frontal area of the models is due to the stagnation point where the  $v_{stag} = 0$  hence induce high pressure on that area as proven by Bernoulli's principle. At the side of the model, the pressure is lower as compared to other parts.

This related to the increase in velocity of the fluid flow across the body. The velocity of fluid increase at the side of the model is due to the increase in distance covered by the fluid. Hence resulting in lower pressure formed.

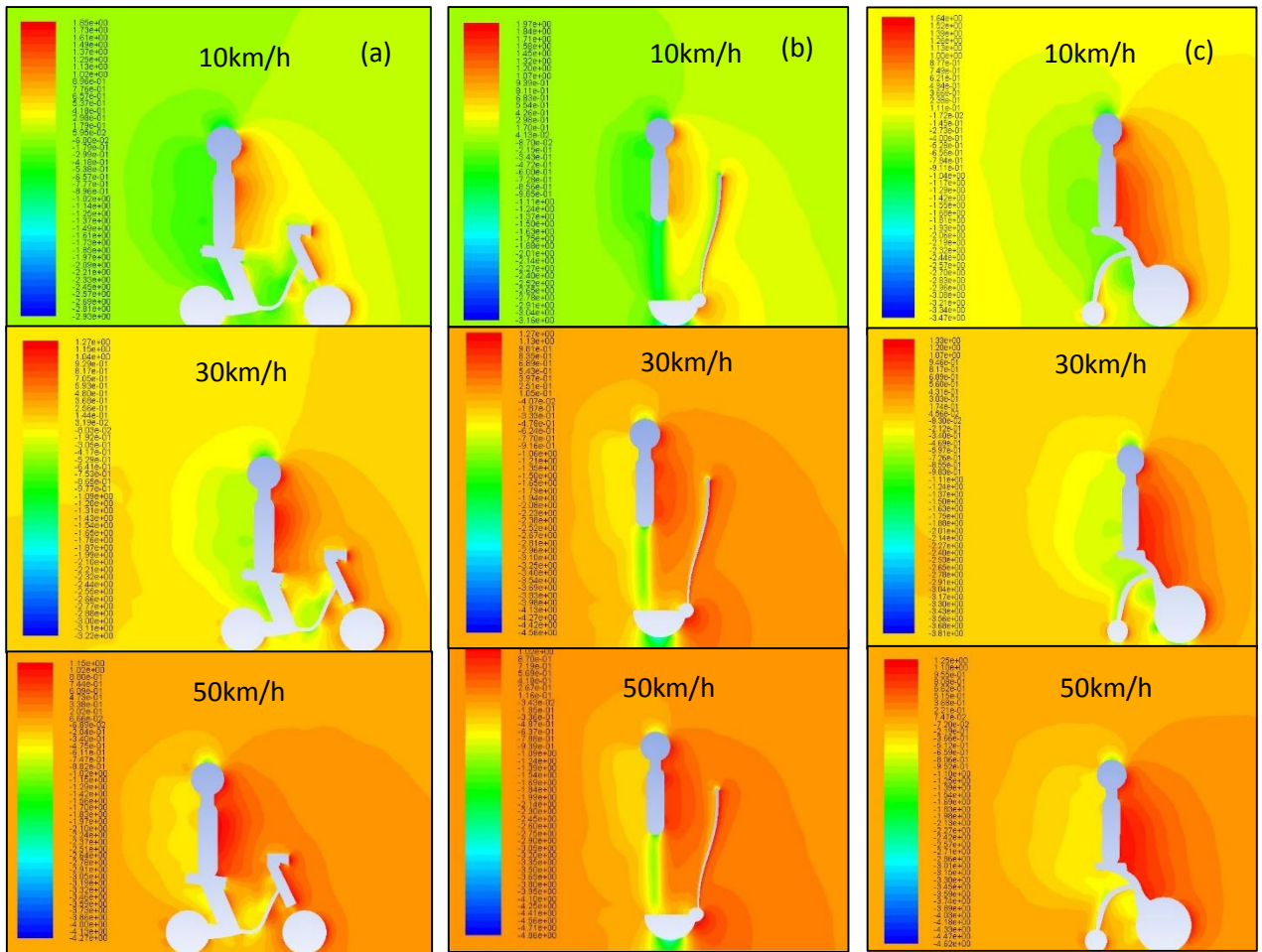


Figure 12: Pressure coefficient on mid cross section plane. (a) Passol; (b) Segway; (c) YikeBike

Figure 12 shows the contour of pressure coefficient around the model at speed of 10 km/h, 30 km/h and 50 km/h which is computed from the symmetry plane define at the middle cross section. The graphical data clearly show the area of overpressure in front of the models and the area of under pressure behind them. For every model, the extent of overpressure area in front of the model increase as the speed of the model increase.

At speed 10 km/h, the extent of the overpressure area in front of the model is the highest for YikeBike as compared to Segway and Passol. This is due to the larger frontal area of the YikeBike model which subsequently induced greater extent of area under pressure behind the model. The area of under pressure around the model can cause turbulence to be formed which can add more drag to the model. Note that, as the speed of PEV increases, the coefficient pressure decreases (Appendix A). This is

caused by increase in velocity of fluid flow resulting in decrease in pressure. Subsequently, the pressure drag force induced increase exponentially with respect to velocity as shown in Figure 13.

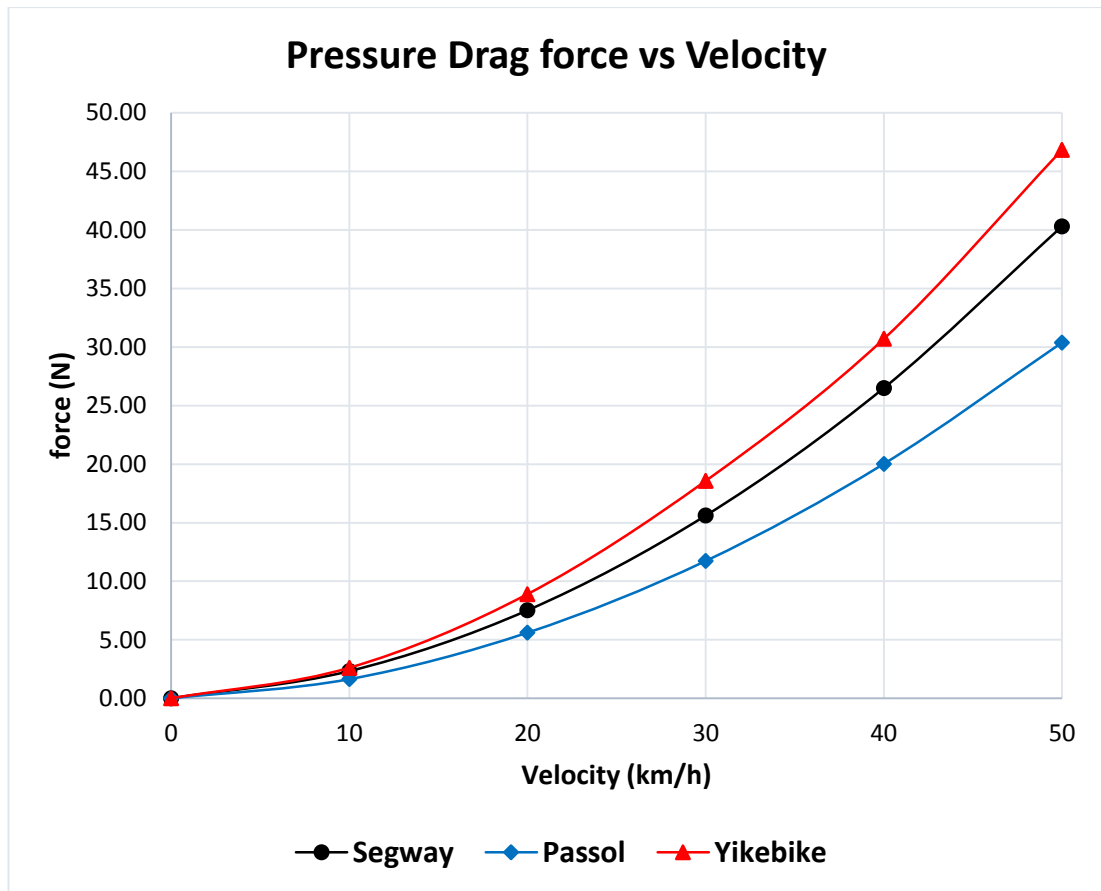


Figure 13: Pressure drag force induce by the models respect to velocity

## CHAPTER 5: CONCLUSION AND RECOMMENDATION

### 5.1 Conclusion

In general, the coefficient of drag is the summation coefficient of pressure drag, skin friction drag, interference drag, lift drag or known as downforce and wave drag. Since PEV does not have streamline and aerodynamic shape and moving at speed up to 50 km/h subsequently induce very small value of lift force and interference drag force which are neglected in this study. Apart from that, wave drag also is neglected in this study since PEV move at low speed leaving only pressure drag and skin friction drag as shown in Equation 5.

$$C_d = C_{pressure} + C_{skin} \quad (5)$$

As comparison to YikeBike, Passol have a drag reduction of 58.0%, 56.6%, 56.3%, 51.4% and 52.3% respectively for the speeds of 10 km/h, 20 km/h, 30 km/h, 40 km/h and 50 km/h respectively. For Segway, the drag reduction is 10.3%, 16.4%, 17.0%, 14.1% and 14.5% respectively as compared to YikeBike. Passol model have the highest drag force reduction as shown in Figure 8 which prove that, Passol is the most aerodynamic model followed by Segway and YikeBike. A number of important conclusions can be stated as follow:

- Passol have the best design in term of aerodynamic drag followed by Segway and yikeBike
- The pressure distribution around the model is affected by the speed of the wind flow which is explained by the theory of Bernoulli principle.
- The posture of the rider involve in this study are sitting (Passol) and standing (Segway, YikeBike). The result of this simulation is supported by [12] where sitting position have the lowest Cd value which is 0.7 compared to standing position 1.2.

## 5.2 Recommendation

Note that, only CFD simulation is done to compute this air drag study and wind tunnel testing for the models is not conducted. Here are some of the advantages of CFD simulation as compared to wind tunnel testing.

Table 7: Wind tunnel and CFD comparison

<b>Wind tunnel testing</b>	<b>CFD simulation</b>
Expensive running cost	Cheaper running cost
Time consuming	Change can be made easily
Need physical model	CAD model is needed
Visualization wind using smoke	Visualization line and arrow vector
Noise	No noise
Not effective for small scale change	Effective for almost all sizes of model

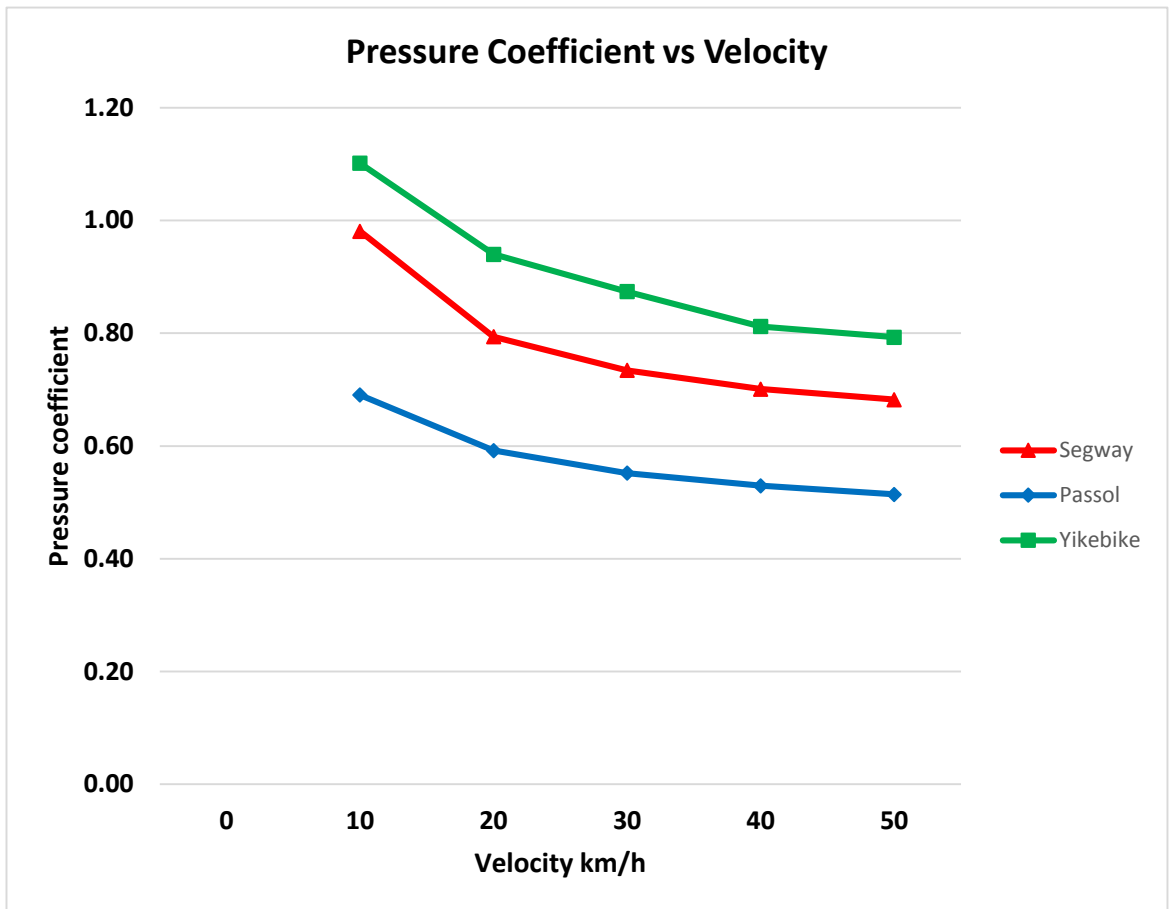
However, it is important to compute the wind tunnel testing and CFD simulation to compare the result and percentage different for the validation of data. Below are some of the recommendations for future study on air drag of PEV:

- CAD models based on actual dimension of PEV available on market
- Use high resolution 3D laser scanning to capture the specific body characteristic on real model
- Compare the result with wind tunnel testing
- Improve the meshing quality for all models
- Run simulation separately for rider and PEV
- Use full model

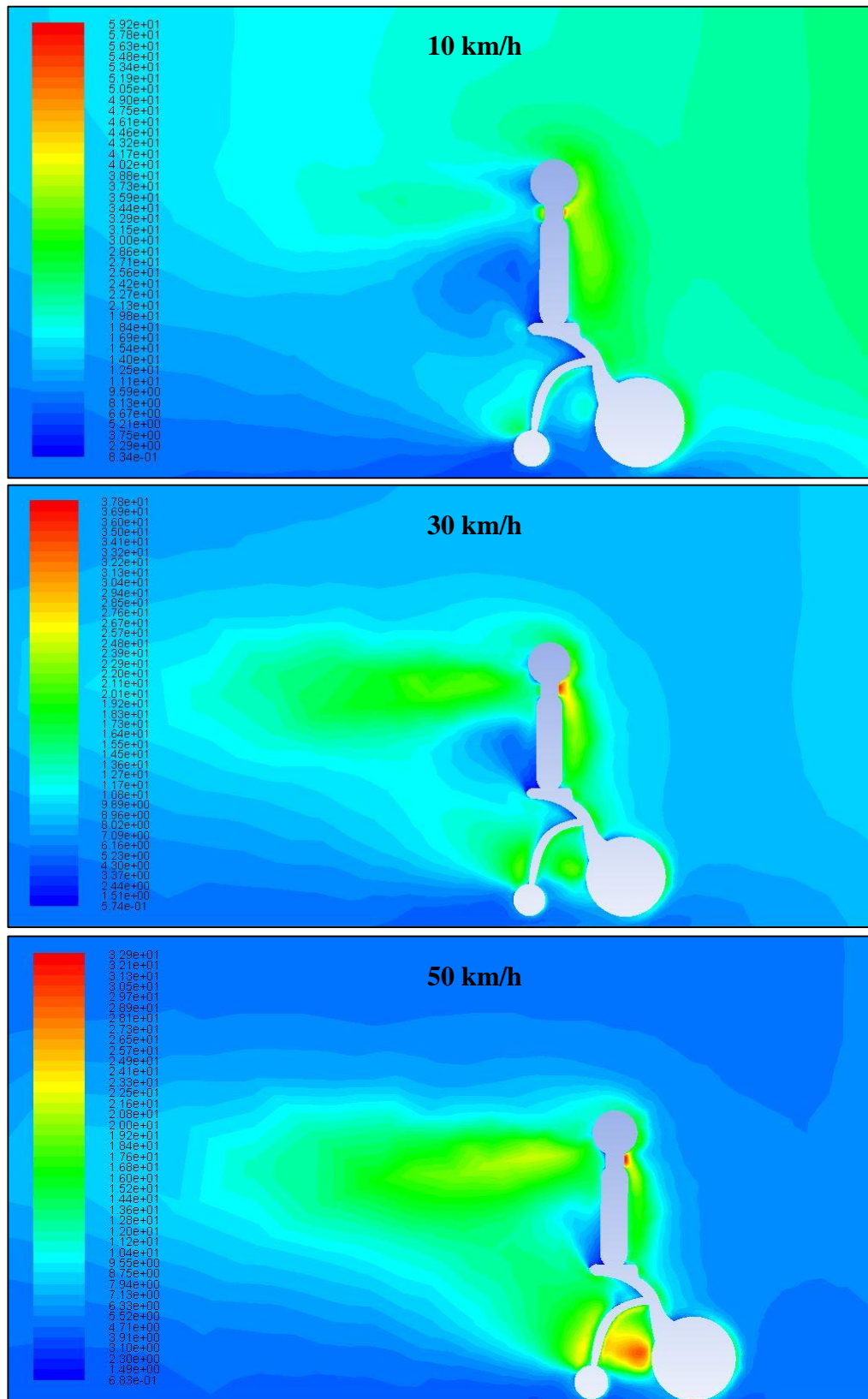
## REFERENCES

- [1] G. Maggetto and J. V. Mierlo, "Electric and electric hybrid vehicle technology: a survey," in *IEE Seminar*, Durham, 2000.
- [2] K. T. Ulrich, "Estimating the technology frontier for personal electric vehicles," *Transportation Research*, vol. Part C, no. 13, pp. 448-462, 2006.
- [3] K. CR and B. ER, "Improving the racing bicycle," *Mech Eng*, vol. 106, no. 9, p. 34–45, 1984.
- [4] R. Faria, P. Moura, J. Delgado and A. T. d. Almeida, "A sustainability assessment of electric vehicles as a personal mobility system," *Energy Conversion and Management*, vol. 61, pp. 19-30, 2012.
- [5] B. Blocken, T. Defraeye, E. Koninckx, J. Carmeliet and P. Hespel, "CFD simulations of the aerodynamic drag of two drafting cyclists," *Computers & Fluids*, vol. 71, pp. 435-445, 2013.
- [6] "Dimensions of a Segway," DimensionsInfo, 18 November 2009. [Online]. Available: <http://www.dimensionsinfo.com/dimensions-of-a-segway/>. [Accessed 5 April 2015].
- [7] "Yamaha Passol," Wikipedia, 2 march 2015. [Online]. Available: [http://en.wikipedia.org/wiki/Yamaha\\_Passol](http://en.wikipedia.org/wiki/Yamaha_Passol). [Accessed 5 April 2015].
- [8] "Yike Bike," TECH VEHI, [Online]. Available: <http://www.technologicvehicles.com/en/details/742/yike-bike-fusion-prix-et-fiche-technique#>. [Accessed 5 April 2015].
- [9] T. Defraeye, B. Blocken, E. Koninckx, P. Hespel and J. Carmeliet, "Computational fluid dynamics analysis of cyclist aerodynamics: Performance of different turbulent-modelling and boundary-layers modelling approaches," *Journal of Biomechanics*, vol. 43, p. 2281–2287, 2010.
- [10] M. P. Bulat and P. V. Bulat, "Comparison of Turbulence Models in the Calculation of Supersonic Separated Flows," *World Applied Sciences Journal*, vol. 27, no. 10, pp. 1263-1266, 2013.
- [11] "SIMPLE algorithm," Wikipedia, 4 March 2015. [Online]. Available: [http://en.wikipedia.org/wiki/SIMPLE\\_algorithm](http://en.wikipedia.org/wiki/SIMPLE_algorithm). [Accessed 11 April 2015].
- [12] M. H. Koo and A. S. M. Al-Obaidi, "Calculation of Aerodynamic Drag of Human Being in Various Positions," *EURECA*, pp. 99-100, 2013.

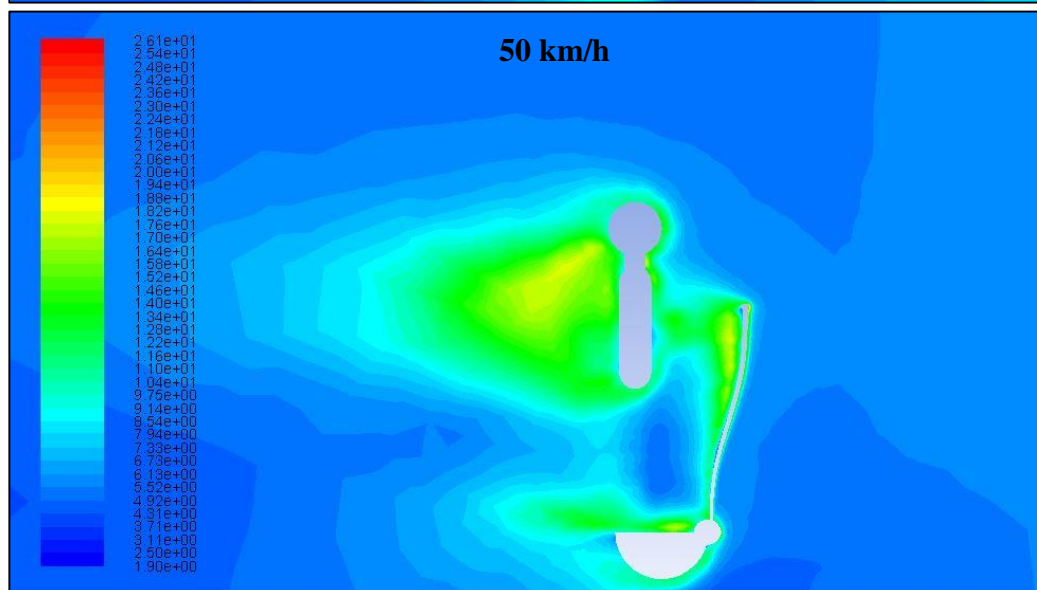
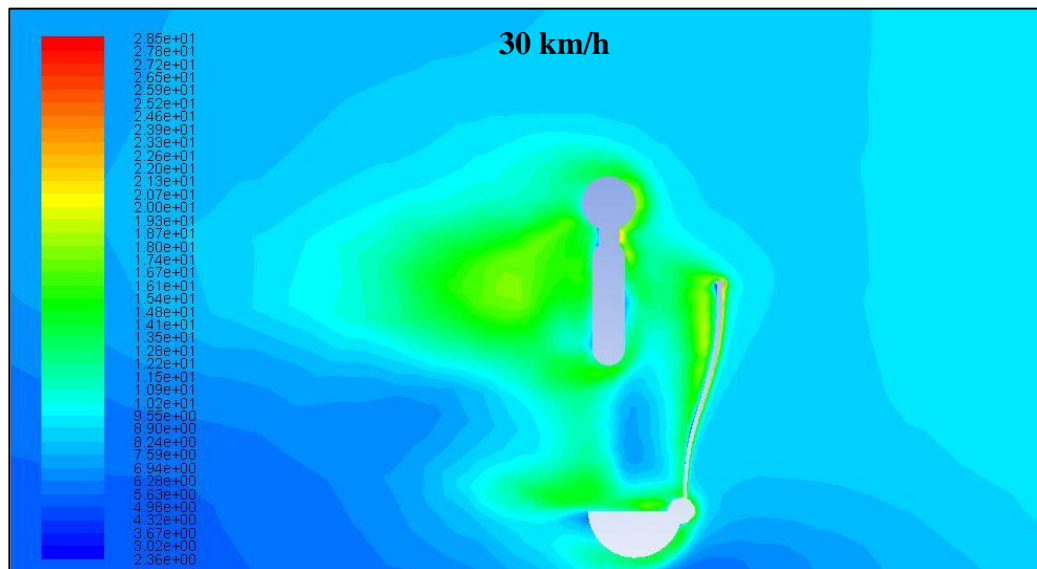
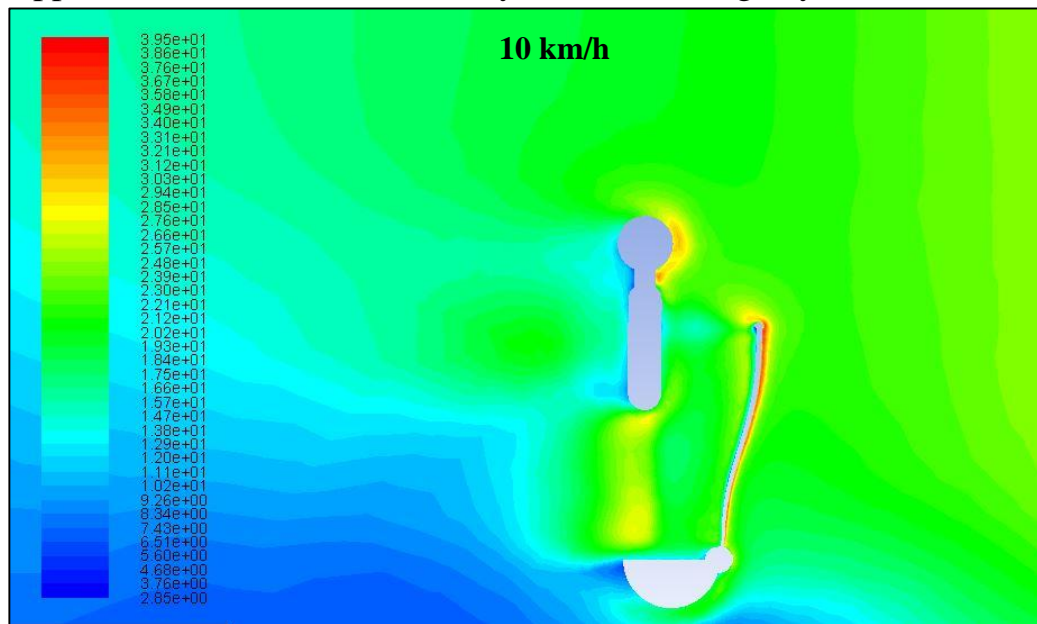
## Appendix A: Pressure Coefficient vs Velocity



## Appendix B: Turbulence Intensity Contour of YikeBike



## Appendix C: Turbulence Intensity Contour of Segway



## Appendix D: Turbulence Intensity Contour of Passol

